Molecular packing and intermolecular interactions in two structural polymorphs of *N*-palmitoylethanolamine, a type 2 cannabinoid receptor agonist

Ravi Kanth Kamlekar and Musti J. Swamy[1]

School of Chemistry, University of Hyderabad, Hyderabad 500 046, India

Abstract **The molecular structure, packing properties, and intermolecular interactions of two structural polymorphs of *N*-palmitoylethanolamine (NPEA) have been determined by single-crystal X-ray diffraction. Polymorphs α and β crystallized in monoclinic space group $P2_1/c$ and orthorhombic space group *P*bca, respectively. In both polymorphs, NPEA molecules are organized in a tail-to-tail manner, resembling a bilayer membrane. Although the molecular packing in polymorph α is similar to that in *N*-myristoylethanolamine and *N*-stearoylethanolamine, polymorph β is a new form. The acyl chains in both polymorphs are tilted by ~35° with respect to the bilayer normal, with their hydrocarbon moieties packed in an orthorhombic subcell. In both structures, the hydroxy group of NPEA forms two hydrogen bonds with the hydroxy groups of molecules in the opposite leaflet, resulting in extended, zig-zag type H-bonded networks along the *b*-axis in polymorph α and along the *a*-axis in polymorph β. Additionally, the amide N-H and carbonyl groups of adjacent molecules are involved in N-H···O hydrogen bonds that connect adjacent molecules along the *b*-axis and *a*-axis, respectively, in α and β. Whereas in polymorph α the L-shaped NPEA molecules in opposite layers are arranged to yield a Z-like organization, in polymorph β one of the two NPEA molecules is rotated 180°, leading to a W-like arrangement. Lattice energy calculations indicate that polymorph α is more stable than polymorph β by ~2.65 kcal/mol.**—Kamlekar, R. K. and M. J. Swamy. **Molecular packing and intermolecular interactions in two structural polymorphs of *N*-palmitoylethanolamine, a type 2 cannabinoid receptor agonist. *J. Lipid Res.* 2006.** 47: **1424–1433.**

Supplementary key words *N*-acylethanolamine • hydrogen bonding • single-crystal X-ray diffraction • chain packing • bilayer membrane

N-Acylethanolamines (NAEs) are naturally occurring amphiphilic derivatives of 2-ethanolamine, wherein the amino group is derivatized with a long acyl chain. They appear to be ubiquitous molecules, with their presence in a wide variety of animals, plants, and microbes such as bacteria, fungi, and viruses being well established (1, 2). The content of long-chain NAEs and their precursors, *N*-acylphosphatidylethanolamines (NAPEs), increases quite dramatically in the parent organisms under conditions of stress (3). For example, both NAEs and NAPEs accumulate in animal tissues during stress conditions such as postdecapitative ischemia in rat brain (4, 5) and traumatic brain injury (6, 7), and their content increases to very high levels when extensive membrane degradation occurs, such as in myocardial infarction (1, 3, 8–11). They also accumulate in a variety of human tumors and surrounding normal tissues. Because NAEs have been also shown to inhibit the growth of different cell lines in vitro, this observation suggests that their accumulation in the tumor tissue may be attributable to the production of NAEs by the adjacent tissues to fight the cancerous growth (12). These observations have led to the postulate that increases in the levels of NAEs and NAPEs probably are attributable to a stress-fighting response of the parent organisms.

Besides their increased levels in various organisms under conditions of stress, NAEs also exhibit several interesting biological and medicinal properties. It has been shown that *N*-arachidonylethanolamine (anandamide) acts as an endogenous ligand of type I cannabinoid receptors, inhibits gap-junction conductance, and reduces the fertilizing capacity of sperm (13–15), whereas *N*-palmitoylethanolamine (NPEA) acts as an agonist for the type 2 cannabinoid receptor CB-2 (16). *N*-Myristoylethanolamine (NMEA) and *N*-lauroylethanolamine are secreted into the culture medium of tobacco cells when challenged by the fungal elicitor xylanase (17). NAEs also exhibit anti-inflammatory, antibacterial, and antiviral properties, which have considerable application potential (1, 18).

Besides the interesting biological properties exhibited by them, NAEs and NAPEs may also be useful in developing liposomal formulations for drug delivery and targeting, in view of their ability to stabilize bilayer structure; especially, *N*-palmitoyl phosphatidylethanolamine has been

Manuscript received 27 January 2006 and in revised form 7 April 2006.

Published, JLR Papers in Press, April 11, 2006.
DOI 10.1194/jlr.M600043-JLR200

[1] To whom correspondence should be addressed.
e-mail: mjssc@uohyd.ernet.in

shown to stabilize liposomes even in the presence of human serum (19–21).

In view of their interesting biological properties, putative role in the stress-combating response of organisms, therapeutic potential in treating bacterial, fungal, and viral infections, and potential in developing liposomal drug-delivery vehicles, it is important to carry out systematic investigations on NAEs and NAPEs directed at understanding their metabolism, physicochemical properties (e.g., phase transitions and supramolecular structure), and interaction with other membrane lipids and proteins. Considerable work has already been done on the metabolism of NAPEs and NAEs, and it has been shown that the former are continuously synthesized by a calcium- and energy-dependent transacylase and are hydrolyzed by a phospholipase D-type enzyme to phosphatidic acid and NAEs, which are further degraded by fatty acid amidohydrolase (3, 22). More recently, it has been demonstrated that NPEA and anandamide can also be synthesized by the sequential action of phospholipase A_2 and lysophospholipase D on NAPEs (23). Several of these enzymes involved in the biosynthesis and degradation of NAPEs and NAEs have been purified, characterized, and cloned (23–25).

In earlier studies, we investigated the chain-melting phase transitions of homologous series of these two classes of compounds by differential scanning calorimetry (DSC), which indicated that the longer chain length NAEs exhibit one or two minor transitions before the main chain-melting phase transition, suggesting that they exhibit structural polymorphism in the solid state (8, 26–28). Additionally, we have also reported the crystal structure of NMEA and analyzed the intermolecular interactions and molecular packing in the crystal lattice (29). Studies using DSC, fast-atom bombardment mass spectrometry, and computational modeling have indicated that NMEA forms a 1:1 (mol/mol) complex with cholesterol (30). In another study, the interaction of NPEA with dipalmitoylphosphatidylcholine was investigated by DSC, ^{31}P-NMR, and small-angle X-ray scattering (31). Here, we report single-crystal X-ray diffraction studies on two structural polymorphs of NPEA (designated α and β) and analyze the molecular packing and intermolecular interactions in the crystal lattice. Although in both polymorphs the molecular structure of NPEA is similar to that observed earlier with NMEA and *N*-stearoylethanolamine (NSEA), in the β polymorph, which is a new crystal form of NAE, the molecules pack in a different way. However, the hydrogen bonding pattern is remarkably similar in both forms.

MATERIALS AND METHODS

Materials

Palmitic acid was purchased from Sigma (St. Louis, MO). Oxalyl chloride was from Merck. Ethanolamine was obtained from Ranbaxy (Mumbai, India). Palmitic acid was converted to palmitoyl chloride by treating with 4 mol equivalents of oxalyl chloride according to the procedure described previously (32). NPEA was synthesized by the reaction of palmitoyl chloride with ethanolamine and characterized by thin-layer chromatography and infrared spectroscopy as reported earlier (26). All solvents were distilled and dried before use.

Crystallization and X-ray diffraction

Thin plate-type colorless crystals of NPEA were grown at room temperature from isobutanol. A crystal of 0.03 × 0.42 × 0.50 mm was used for the data collection. Diamond-shaped, colorless crystals of NPEA were grown at room temperature from a 1:1 (v/v) mixture of dichloromethane and toluene containing a trace of ethanol. A crystal of 0.24 × 0.14 × 0.12 mm was used for data collection in this study. As will be discussed below, these two types of crystals gave two different polymorphic structures. Therefore, henceforth, they will be referred to as polymorph α and polymorph β, respectively. X-ray diffraction measurements were carried out at room temperature (~25°C) with a Bruker SMART APEX charge-coupled device area detector system using a graphite monochromator and Mo-Kα (λ = 0.71073 Å) radiation obtained from a fine-focus sealed tube.

Structure solution and refinement

For polymorphs α and β, the data collected in the range of θ = 1.41−26° and θ = 1.41−25°, respectively, were used for structure solution. Data reduction was done using the Bruker SAINTPLUS program. Structure solution was carried out in the monoclinic space group for α and the orthorhombic space group for β. Absorption correction was applied using the SADABS program. The structures were solved successfully by direct methods in the space groups $P2_1/c$ for α and *P*bca for β. In both cases, refinement was done by full matrix least-squares procedure using the SHELXL97 program (33). For polymorph α, the refinement was carried out using 2,264 observed [$>2\sigma(F_o)$] reflections and converged into a final $R_1 = 0.058$, w$R_2 = 0.1604$ with goodness of fit = 1.032, whereas for polymorph β, 2,679 observed [$>2\sigma(F_o)$] reflections upon refinement converged into a final $R_1 = 0.0978$, w$R_2 = 0.2635$ with goodness of fit = 1.036. For both structures, two hydrogen atoms, the amide N-H and hydroxyl O-H, were refined isotropically, whereas all of the carbon atoms and heteroatoms (N and O) were refined anisotropically. All hydrogen atoms on the acyl chains and other carbon atoms were included in the structure factor calculation with fixed thermal parameters at idealized positions but were not refined.

Crystal parameters of NPEA

Polymorph α. The molecular formula is $C_{18}H_{37}NO_2$; molecular formula weight is 299.49. Crystals were thin plate-type and colorless. The crystal system was monoclinic. Space group, Sg = $P2_1/c$; ambient temperature, T = 298 (2) K; radiation wavelength (λ) = 0.71073 Å; radiation type, Mo-Kα; radiation source, fine-focus sealed tube; radiation monochromator, graphite. Number of reflections collected was 18,314; unique reflections, 3,685. Reflection with $I > 2\sigma(I)$, 2,264; number of parameters, 192.

Unit cell dimensions (with standard deviations in parentheses) are as follows: space group = $P2_1/c$; a = 43.410 (13), b = 4.8850 (15), c = 9.003 (3) Å; β = 94.075 (6); volume of the cell, V = 1,904.4 (10) Å^3 (5); density, D_{Calc} = 1.045 g/cm; number of molecules in the unit cell, Z = 4; angle of tilt of acyl chains, ø = 34.5°; cross-sectional area of the unit cell, Σ = 43.979 Å^2; area per molecule, S = 21.989 Å^2; $F_{(000)}$ = 672; absorption coefficient, μ = 0.066 mm^{-1}; T = 298 (2) K.

Polymorph β. The molecular formula is $C_{18}H_{37}NO_2$. Crystals were colorless and diamond-shaped. Crystal system, orthorhom-

bic; space group, Sg = *P*bca; ambient temperature, T = 298 (2) K; radiation wavelength (λ) = 0.71073 Å; radiation type, Mo-Kα; radiation source, fine-focus sealed tube; radiation monochromator, graphite. Number of reflections collected was 33,801; unique reflections, 3,586. Reflections with $I > 2\sigma(I)$, 2,679; number of parameters, 198.

Unit cell dimensions (with standard deviations in parentheses) are as follows: space group = *P*bca; a = 4.8979 (4), b = 8.9974 (7), c = 86.419 (7) Å; volume of the cell, V = 3,808.3 Å^3 (5); density, D_{Calc} = 1.045 g/cm; number of molecules in the unit cell, Z = 8; angle of tilt of acyl chains, ø = 35.5°; cross-sectional area of the unit cell, Σ = 44.068 Å^2; area per molecule, S = 22.034 Å^2; $F_{(000)}$ = 1,344; absorption coefficient, μ = 0.066 mm^{-1}; T = 298 (2) K.

Lattice energy calculations

Lattice energy calculations for polymorphs α and β were performed using the COMPASS force field in the Cerius^2 suite of programs (Accelrys, Inc., San Diego, CA; http://www.accelrys.com). Lattice energies were reported after normalizing the values obtained for a single molecule.

DSC

Differential scanning calorimetric scans were recorded on a TA Instruments Universal V2.6D differential scanning calorimeter. Samples of dry NPEA (~1–2 mg) were loaded into aluminum sample pans covered with aluminum lids and sealed by crimping. Reference pans were prepared in a similar manner but without any sample in the pan. DSC measurements were performed by heating the samples at a scan rate of 0.5°C/min or 1.5°C/min. Transition enthalpies (ΔH_t) were estimated by integrating the areas under the peaks corresponding to the individual transitions. Transition entropies (ΔS_t) were determined from the transition enthalpies according to the expression (34):

$$\Delta H\mathrm{t} = T_\mathrm{t} \times \Delta S_\mathrm{t}$$

RESULTS AND DISCUSSION

Description of the structure

The molecular structure of NPEA as found in polymorph α is shown in the Oak Ridge thermal ellipsoid plot (ORTEP) plot given in **Fig. 1**, along with atom numbering for all of the nonhydrogen atoms. The atomic coordinates and equivalent isotropic displacement parameters for all nonhydrogen atoms and the two hydrogen atoms on heteroatoms (N-H and O-H) are given in **Table 1**. The bond distances, bond angles, and torsion angles involving all of the nonhydrogen atoms are given in **Tables 2, 3, and 4**, respectively. From the data presented in Table 4, it is seen that the torsion angles observed for the acyl chain region, excepting the C1-C2-C3-C4 angle, which is 68.13°, are all close to 180°, clearly indicating that the hydrocarbon portion (C3-C16) of the acyl chains is in an all-*trans* conformation (Fig. 1). The gauche conformation at the C2-C3 bond results in a bending of the molecule, giving it an L shape. The carbonyl group and the amide N-H are also in *trans* geometry. The molecular structure of NPEA observed here is very similar to the structures of NMEA and NSEA reported previously (29, 35).

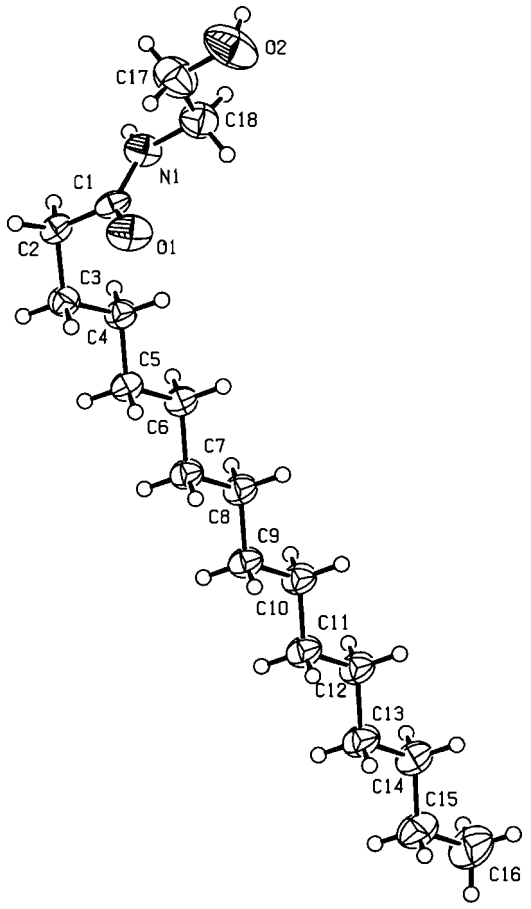

Fig. 1. ORTEP plot of *N*-palmitoylethanolamine (NPEA) in the α polymorph. The atom numbering is indicated. Hatched symbols indicate atoms that are refined anisotropically.

NPEA adopts an essentially similar structure in the β polymorph, which is a new structural form of NAE. Only very minor differences were seen between the molecular features of NPEA in these two polymorphs, although certain distinct differences are seen in the molecular packing between the two polymorphs, which are discussed below. For example, the C1-C2-C3-C4 torsion angle in polymorph β is found to be 66.9°, which is very close to the value of 68.13° mentioned above for polymorph α and the value of 68.5° for the corresponding torsion angle in the crystal structure of NMEA (29). The atomic coordinates and equivalent isotropic displacement parameters for all nonhydrogen atoms in polymorph β are given in **Table 5**. The bond distances, bond angles, and torsion angles involving all of the nonhydrogen atoms are given in **Tables 6, 7, and 8**, respectively.

Molecular packing

Packing diagrams of NPEA along the *c*-axis and *b*-axis in polymorph α are shown in **Fig. 2A, B**, respectively. The NPEA molecules are packed head-to-head (and tail-to-tail) in stacked bilayers. As will be discussed in greater detail below, the hydroxy groups from opposite layers form O-H···O hydrogen bonds, which, together with N-H···O

TABLE 1. Fractional atomic coordinates ($\times 10^4$) and equivalent isotropic displacement parameters ($Å^2 \times 10^3$) for the α form of NPEA

Atom	x	y	z	U(eq)
N(1)	5,884 (1)	8,627 (3)	4,575 (2)	46(1)
O(1)	6,017 (1)	12,984 (2)	4,991 (2)	61(1)
O(2)	5,121 (1)	10,477 (3)	2,808 (2)	94(1)
C(1)	6,051 (1)	10,553 (3)	5,286 (2)	39(1)
C(2)	6,285 (1)	9,599 (3)	6,481 (2)	40(1)
C(3)	6,609 (1)	10,696 (3)	6,273 (2)	41(1)
C(4)	6,755 (1)	9,536 (3)	4,925 (2)	41(1)
C(5)	7,077 (1)	10,634 (3)	4,755 (2)	41(1)
C(6)	7,238 (1)	9,426 (3)	3,457 (2)	42(1)
C(7)	7,559 (1)	10,589 (3)	3,301 (2)	43(1)
C(8)	7,724 (1)	9,388 (4)	2,015 (2)	45(1)
C(9)	8,043 (1)	10,578 (4)	1,864 (2)	45(1)
C(10)	8,211 (1)	9,396 (4)	584 (2)	47(1)
C(11)	8,530 (1)	10,581 (4)	446 (2)	48(1)
C(12)	8,699 (1)	9,399 (4)	−829 (2)	49(1)
C(13)	9,020 (1)	10,577 (4)	−949 (2)	54(1)
C(14)	9,191 (1)	9,424 (4)	−2,219 (2)	54(1)
C(15)	9,511 (1)	10,559 (5)	−2,327 (2)	69(1)
C(16)	9,678 (1)	9,437 (5)	−3,611 (3)	86(1)
C(17)	5,352 (1)	9,975 (5)	3,995 (3)	75(1)
C(18)	5,647 (1)	9,219 (4)	3,379 (2)	58(1)
H(1)	59,166	69,482	48,281	55
H(2)	50,460	90,178	25,132	140

NPEA, *N*-palmitoylethanolamine. U(eq) is defined as one-third of the trace of the orthogonalized Uij tensor [$U(eq) = {}^1/_3 \Sigma_i \Sigma_j U_{ij} a_i * a_j * a_i a_j \cos(ai, aj)$].

hydrogen bonds between adjacent molecules in the same leaflet, appear to drive the formation of such bilayer-like supramolecular arrangement. The methyl ends of the stacked bilayers are in van der Waals contacts, with the closest methyl-methyl (C16-C16) distance between opposing layers and within the same layer being 3.922 and 4.885 Å, respectively.

The bilayer thickness (O2-O2 distance) in the α polymorph is 45.57 Å, and the all-*trans* acyl chains are tilted by 34.5° with respect to the bilayer normal. This is identical to the tilt angle in NSEA and very close to that observed in NMEA (37°) (29, 35). Other long-chain molecules such as long-chain carboxylic acids and *n*-alcohols also pack in a bilayer form with tail-to-tail hydrocarbon alignment with tilted chains (36).

Packing diagrams corresponding to the β polymorph of NPEA along the *b*-axis and *a*-axis are given in Fig. 2C, D, respectively. Similar to the α polymorph, the NPEA molecules are packed in a tail-to-tail manner akin to that found in a lipid bilayer in this polymorph, with O-H···O hydrogen bonds between the hydroxyl groups from opposite layers. However, a very significant difference is seen in the alignment between the opposing leaflets. Although in polymorph α the L-shaped NPEA molecules in opposite layers are arranged to yield a Z-like shape, in polymorph β one of the two NPEA molecules is rotated by ~180°, such that the organization of two molecules yields a W-like shape. This is shown schematically in **Fig. 3**. Despite this difference in the orientation of the acyl chains with respect to polymorph α, the hydrogen bonding network involving the amide N-H and carbonyl groups of adjacent molecules in polymorph β is remarkably similar to that in polymorph α. In addition, the β form contains eight mol-

TABLE 2. Bond lengths (Å) for the α form of NPEA

O(1)-C(1)	1.2238 (18)
O(2)-C(17)	1.434 (3)
N(1)-C(1)	1.325 (2)
N(1)-C(18)	1.464 (2)
C(1)-C(2)	1.500 (2)
C(2)-C(3)	1.527 (2)
C(3)-C(4)	1.518 (2)
C(4)-C(5)	1.518 (2)
C(5)-C(6)	1.523 (2)
C(6)-C(7)	1.520 (2)
C(7)-C(8)	1.522 (2)
C(8)-C(9)	1.518 (3)
C(9)-C(10)	1.520 (3)
C(10)-C(11)	1.515 (3)
C(11)-C(12)	1.519 (3)
C(12)-C(13)	1.519 (3)
C(13)-C(14)	1.515 (3)
C(14)-C(15)	1.508 (3)
C(15)-C(16)	1.510 (3)
C(17)-C(18)	1.479 (3)

TABLE 3. Bond angles (degrees) for the α form of NPEA

C(1)-N(1)-C(18)	123.17 (15)
O(1)-C(1)-N(1)	122.02 (16)
O(1)-C(1)-C(2)	121.53 (15)
N(1)-C(1)-C(2)	116.45 (13)
C(1)-C(2)-C(3)	112.64 (13)
C(2)-C(3)-C(4)	113.96 (13)
C(3)-C(4)-C(5)	112.88 (13)
C(4)-C(5)-C(6)	114.67 (13)
C(5)-C(6)-C(7)	113.55 (13)
C(6)-C(7)-C(8)	114.21 (14)
C(7)-C(8)-C(9)	113.73 (15)
C(8)-C(9)-C(10)	114.26 (15)
C(9)-C(10)-C(11)	113.96 (15)
C(10)-C(11)-C(12)	114.17 (15)
C(11)-C(12)-C(13)	113.82 (15)
C(12)-C(13)-C(14)	114.46 (15)
C(13)-C(14)-C(15)	114.58 (16)
C(14)-C(15)-C(16)	114.24 (18)
O(2)-C(17)-C(18)	110.00 (2)
N(1)-C(18)-C(17)	110.84 (16)

TABLE 4. Torsion angles (degrees) for the α form of NPEA

C(18)	N(1)	C(1)	O(1)	0.30 (3)
C(18)	N(1)	C(1)	C(2)	−179.80 (15)
C(1)	N(1)	C(18)	C(17)	−83.10 (2)
O(1)	C(1)	C(2)	C(3)	−53.30 (2)
N(1)	C(1)	C(2)	C(3)	126.84 (15)
C(1)	C(2)	C(3)	C(4)	−68.13 (17)
C(2)	C(3)	C(4)	C(5)	−179.32 (13)
C(3)	C(4)	C(5)	C(6)	177.33 (13)
C(4)	C(5)	C(6)	C(7)	179.23 (13)
C(5)	C(6)	C(7)	C(8)	179.59 (14)
C(6)	C(7)	C(8)	C(9)	179.62 (14)
C(7)	C(8)	C(9)	C(10)	−180.00 (14)
C(8)	C(9)	C(10)	C(11)	−179.65 (15)
C(9)	C(10)	C(11)	C(12)	179.79 (15)
C(10)	C(11)	C(12)	C(13)	−179.41 (15)
C(11)	C(12)	C(13)	C(14)	−179.83 (15)
C(12)	C(13)	C(14)	C(15)	−179.13 (16)
C(13)	C(14)	C(15)	C(16)	−178.98 (18)
O(2)	C(17)	C(18)	N(1)	−178.50 (16)

TABLE 5. Fractional atomic coordinates ($\times 10^4$) and equivalent isotropic displacement parameters ($Å^2 \times 10^3$) for the β form of NPEA

Atoms	x	y	z	U(eq)
O(1)	2,007 (4)	−1,288 (4)	1,998 (1)	68(1)
O(2)	4,617 (9)	823 (6)	2,434 (1)	96(1)
N(1)	6,397 (6)	−956 (4)	2,064 (1)	58(1)
C(1)	4,458 (6)	−1,589 (4)	1,980 (1)	47(1)
C(2)	5,375 (7)	−2,716 (4)	1,863 (1)	47(1)
C(3)	4,296 (7)	−2,398 (4)	1,701 (1)	48(1)
C(4)	5,436 (7)	−1,009 (4)	1,627 (1)	45(1)
C(5)	4,365 (7)	−728 (4)	1,466 (1)	45(1)
C(6)	5,569 (7)	623 (4)	1,385 (1)	45(1)
C(7)	4,425 (7)	892 (4)	1,225 (1)	45(1)
C(8)	5,593 (7)	2,226 (4)	1,142 (1)	47(1)
C(9)	4,436 (7)	2,486 (4)	982 (1)	48(1)
C(10)	5,588 (7)	3,823 (4)	898 (1)	49(1)
C(11)	4,445 (7)	4,062 (4)	737 (1)	49(1)
C(12)	5,584 (8)	5,398 (4)	653 (1)	51(1)
C(13)	4,444 (8)	5,624 (4)	493 (1)	57(1)
C(14)	5,558 (8)	6,947 (4)	406 (1)	57(1)
C(15)	4,482 (10)	7,168 (5)	246 (1)	72(1)
C(16)	5,541 (12)	8,504 (5)	162 (1)	88(2)
C(17)	4,950 (11)	−414 (6)	2,323 (1)	84(1)
C(18)	5,816 (9)	242 (5)	2,178 (1)	72(1)
H(1A)	8,190 (8)	−1,290 (4)	2,010 (0)	5(1)
H(1B)	5,880 (9)	990 (5)	2,470 (1)	6(2)

U(eq) is defined as one-third of the trace of the orthogonalized Uij tensor [$U(eq) = {}^1/_3 \Sigma_i \Sigma_j U_{ij} a_i * a_j * aia_j \cos(ai, aj)$].

ecules of NPEA in the orthorhombic unit cell. This is because the hydrogen bonded leaflets in polymorph β are arranged in two different orientations (as seen in Fig. 2C); whereas the methyl termini of the upper two layers in the unit cell point to the left, the methyl termini of the lower pair of layers point to the right. The distance between the terminal methyl groups (C16-C16) of the bilayer in polymorph β is 3.918 Å, whereas that between adjacent molecules in the same layer is 4.898 Å. These values closely match the corresponding values obtained for the α polymorph, as mentioned above.

In an earlier study, Lambert and coworkers (37) studied the polymorphism of NSEA by DSC, powder X-ray diffraction, and Fourier transform infrared spectroscopy. Although the polymorph observed in the crystal structure of NSEA [which is similar to polymorph α of NPEA (35)] was identified by them as the most stable one, based on powder diffraction and Fourier transform infrared data, they proposed that two other polymorphic forms differ from this form in the chain tilt angles and chain mobility, with the head group region remaining essentially unaltered (see Fig. 6 in 37). Our present results, however, indicate that reorientation of the acyl chain region in one layer with respect to the opposite layer, as shown in Fig. 3, resulting from a rotation of the NAE molecules by 180°, would most likely lead to the conversion of the stable form (polymorph α) to a second form (polymorph β). Although our results are obtained with NPEA, similar conversion is highly likely in the other long-chain NAEs as well, especially NMEA and NSEA for which an equivalent to the α polymorph has been observed by single-crystal X-ray diffraction.

Besides the similarities in the hydrogen bonding patterns between the two polymorphs, the bilayer thickness and angle of tilt of the acyl chains are also very similar. Thus, in polymorph β, the O2-O2 distance is 45.2 Å and matches very well the distance of 45.57 Å observed in

TABLE 6. Bond lengths (Å) for the β form of NPEA

O(1)-C(1)	1.240 (4)
O(2)-C(17)	1.480 (6)
N(1)-C(1)	1.322 (5)
N(1)-C(18)	1.488 (6)
C(1)-C(2)	1.504 (5)
C(2)-C(3)	1.522 (5)
C(3)-C(4)	1.507 (5)
C(4)-C(5)	1.508 (5)
C(5)-C(6)	1.518 (5)
C(6)-C(7)	1.516 (5)
C(7)-C(8)	1.509 (5)
C(8)-C(9)	1.509 (5)
C(9)-C(10)	1.515 (5)
C(10)-C(11)	1.509 (5)
C(11)-C(12)	1.513 (5)
C(12)-C(13)	1.501 (5)
C(13)-C(14)	1.508 (5)
C(14)-C(15)	1.498 (5)
C(15)-C(16)	1.496 (6)
C(17)-C(18)	1.449 (6)

TABLE 7. Bond angles (degrees) for the β form of NPEA

C(1)-N(1)-C(18)	122.3 (3)
O(1)-C(1)-N(1)	122.5 (3)
O(1)-C(1)-C(2)	121.0 (3)
N(1)-C(1)-C(2)	116.5 (3)
C(1)-C(2)-C(3)	113.0 (3)
C(2)-C(3)-C(4)	114.6 (3)
C(3)-C(4)-C(5)	113.6 (3)
C(4)-C(5)-C(6)	115.2 (3)
C(5)-C(6)-C(7)	114.1 (3)
C(6)-C(7)-C(8)	115.1 (3)
C(7)-C(8)-C(9)	114.6 (3)
C(8)-C(9)-C(10)	115.2 (3)
C(9)-C(10)-C(11)	114.7 (3)
C(10)-C(11)-C(12)	114.9 (3)
C(11)-C(12)-C(13)	114.6 (3)
C(12)-C(13)-C(14)	115.5 (3)
C(13)-C(14)-C(15)	116.1 (3)
C(14)-C(15)-C(16)	115.8 (4)
O(2)-C(17)-C(18)	106.8 (4)
N(1)-C(18)-C(17)	109.5 (4)

TABLE 8. Torsion angles (degrees) for the β form of NPEA

C(18)	N(1)	C(1)	O(1)	−4.5 (6)
C(18)	N(1)	C(1)	C(2)	176.2 (3)
C(1)	N(1)	C(18)	C(17)	83.6 (5)
O(1)	C(1)	C(2)	C(3)	53.6 (4)
N(1)	C(1)	C(2)	C(3)	−127.0 (3)
C(1)	C(2)	C(3)	C(4)	66.9 (4)
C(2)	C(3)	C(4)	C(5)	179.2 (3)
C(3)	C(4)	C(5)	C(6)	−177.2 (3)
C(4)	C(5)	C(6)	C(7)	−179.1 (3)
C(5)	C(6)	C(7)	C(8)	−179.8 (3)
C(6)	C(7)	C(8)	C(9)	−179.8 (3)
C(7)	C(8)	C(9)	C(10)	179.9 (3)
C(8)	C(9)	C(10)	C(11)	179.2 (3)
C(9)	C(10)	C(11)	C(12)	179.9 (3)
C(10)	C(11)	C(12)	C(13)	179.8 (3)
C(11)	C(12)	C(13)	C(14)	−179.8 (3)
C(12)	C(13)	C(14)	C(15)	178.7 (3)
C(13)	C(14)	C(15)	C(16)	178.5 (4)
O(2)	C(17)	C(18)	N(1)	175.5 (4)

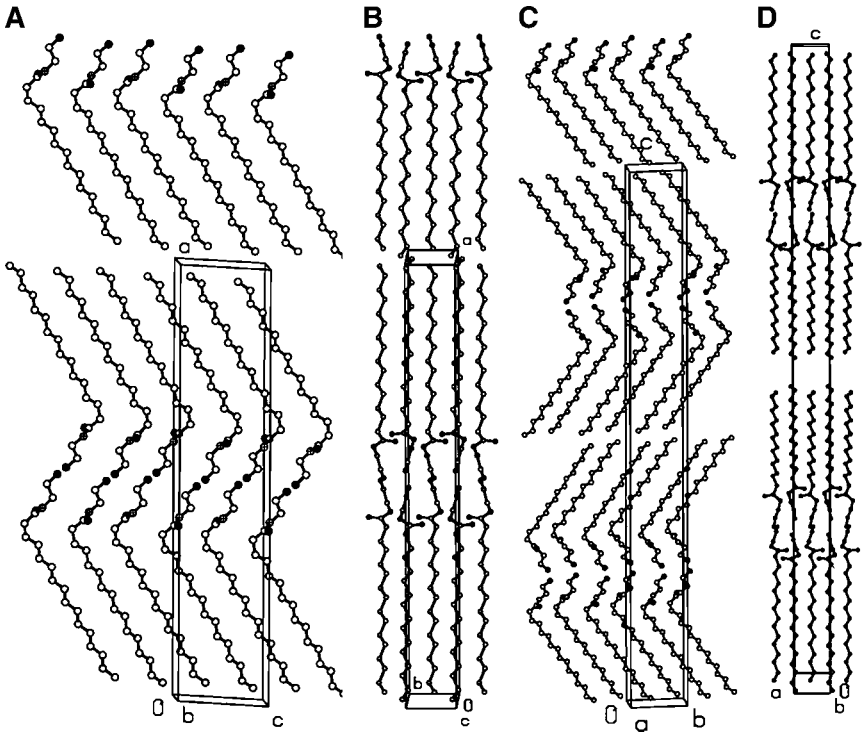

Fig. 2. Packing diagrams of NPEA. A: View along the *c*-axis of polymorph α. B: View along the *b*-axis of polymorph α. C: View along the *b*-axis of polymorph β. D: View along the *a*-axis of polymorph β.

polymorph α, whereas the chain tilt angle of 35.5° for polymorph β is in good agreement with the value of 34.5° estimated for polymorph α.

Subcell structure

The hydrocarbon chains in lipid crystals adopt a variety of lateral packing modes, which may be described by subcells that specify the relations between equivalent positions within the chain and its neighbors. Analysis of a large number of lipid crystal structures has shown that the chain-packing modes fall into a relatively small number of hydrocarbon subcells with triclinic, monoclinic, orthorhombic, and hexagonal symmetry and that their polymethylene planes can be mutually parallel or perpendicular with respect to their neighbors (38, 39). The subcells have been further divided into simple and hybrid types, with the latter type involving more than two different asymmetric units in a subcell. Examination of the hydrocarbon chain packing in the α and β polymorphs of NPEA revealed that the subcells in both of these polymorphs are of the orthorhombic type (O'⊥) in the *P*bnm space group. The unit cell dimensions of these subcells are as follows: a = 7.435 Å, b = 4.885 Å, and c = 2.544 Å for polymorph α and a = 7.45 Å, b = 4.898 Å, and c = 2.547 Å for polymorph β. These then yielded the areas per chain of 18.16 Å^2 for the α polymorph and 18.25 Å^2 for the β polymorph. These parameters are in the range that is typically observed for the orthorhombic type O'⊥ (36).

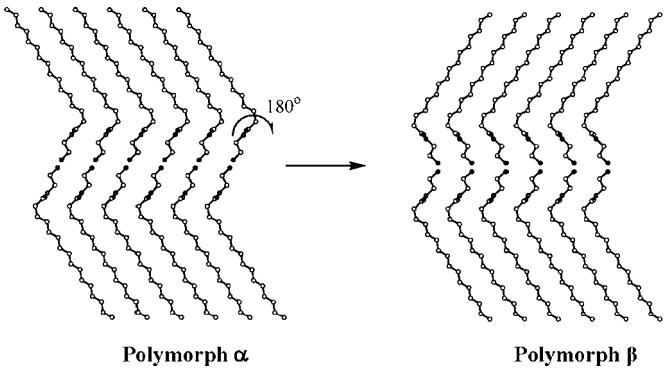

Fig. 3. Model for the interconversion between the α and β polymorphs of NPEA. This model suggests that a simple rotation of all of the molecules in one of the two leaflets of the bilayer by 180° (indicated by the curved arrow) results in the conversion of polymorph α to polymorph β (and vice versa).

Molecular area

The areas per each NPEA molecule in the bilayer plane in the crystal structures of polymorphs α and β are 21.99 and 22.03 Å^2, respectively. These values are in the same range as those found for other NAEs whose three-dimensional structures have been determined, namely NMEA (21.95 Å^2) and NSEA (21.99 Å^2), as well as some other single-chain lipids such as 3(11-bromoundecanoyl)-D-glycerol, 3-lauroyl-D-glycerol, and 3-strearoyl-D-glycerol, whose molecular areas are in the range of 21.5–22.7 Å^2 (29, 35, 40–43). Other single-chain lipids, such as lysophosphatidic acid and lysophosphatidylethanolamine, have somewhat larger molecular areas (33.6 and 34.8 Å^2, respectively). Such large molecular areas observed in these

two molecules are attributable to the very high tilt angle of the acyl chains with respect to the bilayer normal (43–45).

Hydrogen bonding and intermolecular interactions

The molecular packing in the crystal structure of NPEA was examined from various angles to understand the intermolecular interactions. Results obtained for polymorph α, which is similar to the crystal structure of NMEA (29), will be presented first, and then the results from the analysis of polymorph β will be discussed in comparison.

The hydrogen bonding pattern observed in the crystal lattice of polymorph α is shown in **Fig. 4**. Figure 4A gives a view of the molecular packing together with the hydrogen bonds between hydroxyl groups in the opposite leaflets as well as those between the amide hydrogen and the carbonyl oxygen atoms of adjacent layers in the same leaflet of the bilayer. In Fig. 4B, a detailed picture of the hydrogen bonding pattern is shown, viewed along the *b*-axis. The O-H···O hydrogen bonds form an extended, zig-zag-type network along the *b*-axis, with each O-H group being involved in two hydrogen bonds with proximal hydroxyls, one as donor and the other as acceptor. In each unit cell containing four NPEA molecules organized in a bilayer, the hydroxy group of each molecule forms one hydrogen bond within the same unit cell and a second hydrogen bond with another molecule of NPEA in an adjacent unit cell along the *b*-axis. All of the O-H···O hydrogen bonds in the α polymorph are 2.701 (2) Å in length, with the H···O distance and the angle subtended at the hydrogen atom being 1.73 Å and 169°, respectively.

Besides the hydrogen bonds between the hydroxy groups, strong hydrogen bonds are also formed between the amide N-H and carbonyl oxygen of adjacent NPEA molecules along the *b*-axis. The carbonyl oxygen atoms of adjacent molecules point in opposite direction, thus providing the appropriate juxtaposition of the amide carbonyl and hydrogen atoms to interconnect adjacent molecules by hydrogen bonds. All of these hydrogen bonds are again identical, with an N-O distance of 2.836 (2) Å, a H···O distance of 1.84 Å, and an N-H···O angle of 167°.

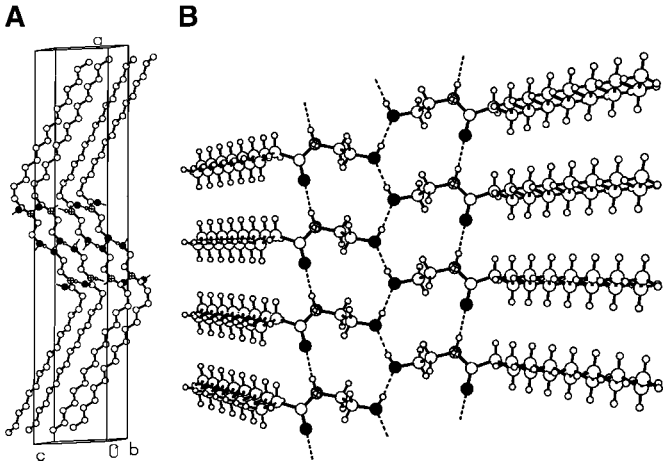

Fig. 4. Hydrogen bonding pattern in the crystal lattice of the α polymorph of NPEA. A: View of the bilayer displaying both the O-H···O and N-H···O type hydrogen bonds. B: Close-up view along the *b*-axis. The hydrogen bonds (N-H···O and O-H···O) are indicated by dashed lines. Small open circles, hydrogen; large open circles, carbon; closed circles, oxygen; hatched circles, nitrogen.

Figure 4B clearly shows that the O-H···O hydrogen bonds form an extended network along the *b*-axis, which stabilizes the bilayer-type packing in the crystal lattice. The hydroxy groups are arranged in a zig-zag network, with the angle between two hydrogen bonds (O2-O2-O2 angle) being 129.5°. This is essentially identical to the value of 129.4° observed for the corresponding O1-O1-O1 angle in the crystal structure of NMEA (29). The N-H···O hydrogen bonds join adjacent NPEA molecules in the same plane along the *b*-axis. Although the N-H group of each NPEA molecule forms a hydrogen bond with another NPEA molecule in the adjacent unit cell on one side, the carbonyl oxygen of the same molecules forms a hydrogen bond with the amide N-H of another NPEA molecule in the adjacent unit cell on the other side (Fig. 4A).

Hydrogen bonding patterns observed in polymorph β are shown in **Fig. 5**. Figure 5A shows both the packing arrangement and hydrogen bonding in polymorph β. In the unit cell containing eight NPEA molecules in two head-to-head bilayers stacked one above the other, the hydroxy group of each molecule forms one hydrogen bond within the same unit cell and a second hydrogen bond with another molecule from one of the adjacent unit cells along the *a*-axis. A comparison of Fig. 5B with Fig. 4B clearly shows that despite the significantly different arrangement of the acyl chains in the opposite leaflets of the bilayer arrangement, the hydrogen bonding pattern in the β polymorph is very similar to that observed in the α polymorph. All of the O-H···O hydrogen bonds in polymorph β of NPEA have the same H···O distance of 1.75 Å, and the distance between the two oxygen atoms is 2.699 (6) Å. These hydrogen bonds are also nonlinear, with the angle between the covalent bond and the hydrogen bond being 160°.

In polymorph β, the hydrogen bonds between the amide N-H and carbonyl oxygen of adjacent NPEA molecules are seen along the *a*-axis. Here, the distance between hydrogen bonded carbonyl oxygen and the amide hydrogen atom is 1.89 Å and the N···O distance is 2.823 (4) Å. The angle between the covalent bond and the hydrogen bond (N-H···O angle) is 152°, which deviates significantly from linearity and hence is expected to be somewhat weaker compared with the N-H···O hydrogen bonds in the α polymorph.

Similar to the α polymorph (Fig. 4B), the O-H···O hydrogen bonds in polymorph β also form extended zig-zag networks (Fig. 5B), which stabilize the bilayer arrangement. These networks are seen along the *a*-axis, and the angle between the two hydrogen bonds (O2-O2-O2 angle) at each oxygen atom is 130.3°. The N-H···O hydrogen bonds connect the adjacent NPEA molecule in the same plane along the *a*-axis. The amide N-H group of each NPEA molecule forms a hydrogen bond with another molecule in the adjacent unit cell on one side, whereas the carbonyl oxygen atom from the same molecule is involved in another hydrogen bond with the amide N-H of an NPEA molecule in the unit cell on the other side (Fig. 5B).

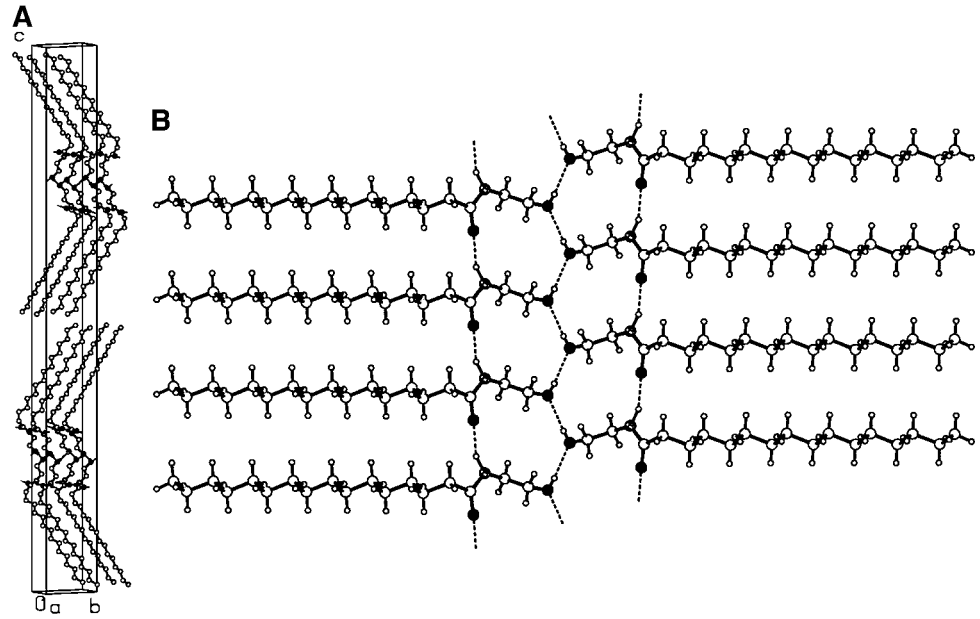

Fig. 5. Hydrogen bonding pattern in the crystal lattice of the β polymorph of NPEA. A: View of the bilayer displaying both the O-H···O and N-H···O type hydrogen bonds. B: Close-up view along the *a*-axis. The hydrogen bonds (N-H···O and O-H···O) are indicated by dashed lines. Small open circles, hydrogen; large open circles, carbon; closed circles, oxygen; hatched circles, nitrogen.

As seen clearly in Figs. 4B and 5B, the interconnecting hydrogen bonds at the head-to-head bilayer interface result in the formation of 14 membered loops. Each loop contains one N-H···O hydrogen bond and two O-H···O hydrogen bonds. Two adjacent molecules of NPEA in each leaflet, which are connected by an N-H···O hydrogen bond, and one NPEA molecule from the opposite leaflet, which forms one hydrogen bond each with these two NPEA molecules via its hydroxy group, are involved in the formation of the 14 membered, hydrogen bonded loop.

Lattice energy calculations

The lattice energy of polymorphs α and β was computed using the COMPASS force field in the Cerius[2] program package to estimate their relative energies. These calculations yielded an overall energy of −46.53 kcal/mol for the α polymorph, which is made up of −39.61 kcal/mol van der Waals energy and −6.92 kcal/mol electrostatic energy. For the β polymorph, the overall computed energy is −43.88 kcal/mol, with the van der Waals and electrostatic components being −39.63 and −4.25 kcal/mol. These results indicate that the crystal lattice energy of polymorph α is lower than that of polymorph β by ∼2.65 kcal/mol, which appears to be arising solely from the electrostatic component. Because the N-H···O bond angle is significantly lower in the β polymorph compared with the α polymorph (167° vs. 152°), it is likely that this difference can be largely accounted for by the weaker N-H···O hydrogen bond in the former.

DSC

Previous DSC studies from this laboratory have shown that, based on the thermal history, NPEA and other long-chain NAEs give one or two minor transitions before the major chain-melting transition, which were attributed to solid-solid phase transitions, indicating structural polymorphism (29). To investigate this further, additional DSC experiments were carried out. Thermogram a in **Fig. 6** gives the first heating scan of the α form of dry NPEA, and thermogram b gives the cooling scan obtained immediately

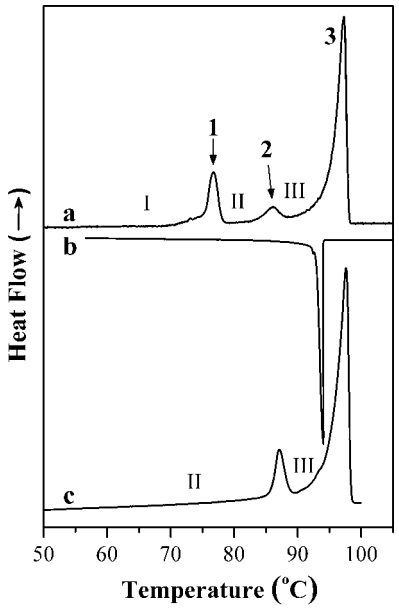

Fig. 6. Differential scanning calorimetric thermograms of the α polymorph of NPEA. Thermogram a: First heating scan. Thermogram b: Cooling scan. Thermogram c: Second heating scan performed in succession.

after the heating. Thermogram c corresponds to the second heating scan of the same sample. The first heating scan shows three endothermic transitions at ~76.8, 86.2, and 97.3°C, with enthalpies of 3.1, 1.3, and 11.3 kcal/mol, respectively, and the enthalpy of transition 3 is in good agreement with the value of 11.54 kcal/mol reported previously for the melting transition of NPEA (29). These results show that NPEA exists in at least three polymorphic forms in the solid state: polymorph I exists below transition 1, polymorph II exists between transitions 1 and 2, and polymorph III exists between transitions 2 and 3. Because the DSC scans were performed with the α polymorph, these results establish that polymorph I is the same as the α form. Heating the α polymorph to 80°C and 90°C (i.e., to temperatures above transitions 1 and 2, respectively), followed by cooling to room temperature and then reheating, gave thermograms that are identical to thermogram c (Fig. 6). This shows that transition 1 is not reversed once it is completed irrespective of whether transitions 2 and 3 are also completed, whereas transition 2 could be readily reversed by cooling from a temperature below transition 3 or above it. These observations suggest the polymorph II is metastable at room temperature.

The enthalpy value of 3.1 kcal/mol for transition 1 occurring at ~77°C (thermogram a, Fig. 6) is in good agreement with the energy difference of 2.65 kcal/mol between the α and β polymorphs obtained from lattice energy calculations described above and suggests that polymorph II is most likely the β form.

It has been suggested that NAEs may stabilize the bilayer structure of diacyl phosphatidylethanolamines because the addition of NAEs, such as *N*-lauroylethanolamine and *N*-oleoylethanolamine, to egg phosphatidylethanolamine shifted its bilayer-inverse hexagonal phase transition to higher temperatures (19). This study, together with earlier studies on the crystal structures of NMEA and NSEA, suggests that such stabilization is probably driven by the strong tendency of the NAEs to form a bilayer structure. This is further strengthened by the observation of bilayer arrangement in both the polymorphic forms of NPEA. Because intermolecular hydrogen bonds between the head groups of neighboring molecules are found in the crystal structures of phosphatidylethanolamines (43, 44) as well as in all of the NAEs for which crystal structures are known, namely NMEA (29), NSEA (35), and NPEA (this study), it appears likely that hydrogen bond formation between phosphatidylethanolamine and NAE may play an important role in such stabilization. Currently, we are investigating the mixing properties of NAEs and phosphatidylethanolamines to understand their interaction at the molecular level.

Conclusions

The crystal structure of NPEA has been solved in two different polymorphic forms (α and β) by single-crystal X-ray diffraction. In both polymorphs, the NPEA molecules adopt a bilayer-type arrangement with tail-to-tail chain packing. This supramolecular organization is governed primarily by strong intermolecular hydrogen bonds between the hydroxy groups of NPEA molecules in opposite leaflets as well as between the amide N-H and C=O groups of adjacent molecules in the same leaflet, with the van der Waals forces between acyl chains providing further stabilization. Although the molecular structure as well as the crystal packing arrangement of NPEA in polymorph α with the $P2_1/c$ space group are very similar to the corresponding features in the crystal structures of NMEA and NSEA reported previously, the crystal packing of NPEA molecules in polymorph β with the *P*bca space group, which is a new form, differs from that in polymorph α. In polymorph α, the supramolecular organization of the bent NPEA molecules in opposite layers yields a Z-like shape, whereas in polymorph β, one of the two NPEA molecules in this organization is rotated by ~180°, such that the two molecules are now arranged in a W shape. Despite these differences, the hydrogen bonding patterns in the two polymorphs are very similar. Packing energy calculations indicate that the α polymorph is more stable than the β polymorph by ~2.65 kcal/mol, which is comparable to the enthalpy of transition 1 seen in the DSC thermograms of the α form of dry NPEA. Finally, this study firmly establishes the existence of different polymorphic forms in NAEs, which was suggested earlier based on DSC studies, and provides a comparison of the structures of two polymorphic forms of NPEA together with a possible mechanism for their interconversion.

This work was supported by a research project from the Department of Science and Technology to M.J.S. (SP/SO/D-124/98). R.K.K. is a Senior Research Fellow of Council of Scientific and Industiral Research (CSIR) (India). Use of the National Single Crystal Diffractometer Facility (SMART APEX CCD single crystal X-ray diffractometer) at the School of Chemistry, University of Hyderabad, funded by the Department of Science and Technology, is gratefully acknowledged. The authors thank the University Grants Commission (India) for its support through the University with Potential for Excellence (UPE) and Centre for Advanced Study (CAS) programs to the University of Hyderabad and the School of Chemistry, respectively, and acknowledge the help of Mr. P. Raghavaiah in X-ray diffraction data collection. The authors are grateful to Prof. Samudranil Pal of this school for advice in X-ray data analysis and to Dr. B. Gopalakrishnan (Tata Consultancy Services, Hyderabad) for helpful suggestions and for critically reading the manuscript.

REFERENCES

1. Schmid, H. H. O., P. C. Schmid, and V. Natarajan. 1990. *N*-Acylated glycerophospholipids and their derivatives. *Prog. Lipid Res.* **29:** 1–43.
2. Hansen, H. S., B. Moesgaard, H. H. Hansen, and G. Petersen. 2000. *N*-Acylethanolamines and precursor phospholipids—relation to cell injury. *Chem. Phys. Lipids.* **108:** 135–150.
3. Schmid, H. H. O., P. C. Schmid, and V. Natarajan. 1996. The *N*-acylation-phosphodiesterase pathway and signalling. *Chem. Phys. Lipids.* **80:** 133–142.
4. Natarajan, V., P. C. Schmid, and H. H. O. Schmid. 1986. *N*-Acylethanolamine phospholipid metabolism in normal and ischemic rat brain. *Biochim. Biophys. Acta.* **878:** 32–41.
5. Moesgaard, B., J. W. Jaroszweski, and H. S. Hansen. 1999. Accu-

mulation of N-acyl-ethanolamine phospholipid in rat brains during post-decapitative ischemia: a ^{31}P NMR study. *J. Lipid Res.* **40:** 515–521.
6. Hansen, H. H., C. Ikonomidou, P. Bittigau, and H. S. Hansen. 2001. Accumulation of the anadamide precursor and other N-acylethanolamine phospholipids in infant rat models of *in vivo* necrotic and apoptotic neural death. *J. Neurochem.* **76:** 39–46.
7. Hansen, H. H., P. C. Schmid, P. Bittigau, I. Lastres-Becker, F. Berrendero, J. Manzanares, C. Ikonomidou, H. H. O. Schmid, J. J. Fernandez-Ruiz, and H. S. Hansen. 2001. Anandamide, but not 2-arachidonoylglycerol, accumulates during *in vivo* neurodegeneration. *J. Neurochem.* **78:** 1415–1427.
8. Marsh, D., and M. J. Swamy. 2000. Derivatised lipids in membranes. Physico-chemical aspects of *N*-biotinyl phosphatidylethanolamines, *N*-acylphosphatidylethanolamines and *N*-acylethanolamines. *Chem. Phys. Lipids.* **105:** 43–69.
9. Chapman, K. D. 2000. Emerging physiological roles for *N*-acylphosphatidylethanolamine metabolism in plants: signal transduction and membrane protection. *Chem. Phys. Lipids.* **108:** 221–230.
10. Epps, D. E., P. C. Schmid, V. Natarajan, and H. H. O. Schmid. 1979. *N*-Acylethanolamine accumulation in infarcted myocardium. *Biochem. Biophys. Res. Commun.* **90:** 628–633.
11. Epps, D. E., V. Natarajan, P. C. Schmid, and H. H. O. Schmid. 1980. Accumulation of *N*-acylethanolamine glycerophospholipids in infarcted myocardium. *Biochim. Biophys. Acta.* **618:** 420–430.
12. Schmid, H. H. O., P. C. Schmid, and E. V. Berdyshev. 2002. Cell signaling by endocannabinoids and their congeners: questions of selectivity and other challenges. *Chem. Phys. Lipids.* **121:** 111–134.
13. Devane, W. A., L. Hanus, A. Breuer, R. G. Pertwee, L. A. Stevensen, G. Griffin, D. Gibson, A. Mandelbaum, A. Etinger, and R. Mechoulam. 1992. Isolation and structure of a brain constituent that binds to the cannabinoid receptor. *Science.* **258:** 1946–1949.
14. Scheul, H., E. Goldstein, R. Mechoulam, A. M. Zimmerman, and S. Zimmerman. 1994. Anandamide (arachidonylethanolamide), a brain cannabinoid receptor agonist, reduces sperm fertilizing capacity in sea urchins by inhibiting the acrosome reaction. *Proc. Natl. Acad. Sci. USA.* **91:** 7678–7682.
15. Venance, L., D. Piomelli, J. Glowinski, and C. Giaume. 1995. Inhibition of anandamide of gap junctions and intercellular calcium signaling in striatal astrocytes. *Nature.* **376:** 590–594.
16. Facci, L., R. Dal Toso, S. Romanello, A. Buriani, S. D. Skaper, and A. Leon. 1995. Mast cells express a peripheral cannabinoid receptor with differential sensitivity to anandamide and palmitoylethanolamide. *Proc. Natl. Acad. Sci. USA.* **92:** 3376–3380.
17. Chapman, K. D., S. Tripathy, B. Venables, and A. D. Desouja. 1998. *N*-Acylethanolamines: formation and molecular composition of a new class of plant lipids. *Plant Physiol.* **116:** 1163–1168.
18. Ganley, O. H., O. E. Graessle, and H. J. Robinson. 1958. Anti-inflammatory activity of compounds obtained from egg yolk, peanut oil, and soybean lecithin. *J. Lab. Clin. Med.* **51:** 709–714.
19. Ambrosoni, A., E. Bertoli, P. Mariani, E. Tanfani, M. Wozniak, and G. Zolese. 1993. *N*-Acylethanolamines as membrane topological stress compromising agents. *Biochim. Biophys. Acta.* **1148:** 351–355.
20. Domingo, J., M. Mora, and M. A. De Madariaga. 1993. Incorporation of *N*-acylethanolamine phospholipids into egg phosphatidylcholine vesicles: characterization and permeability properties of the binary systems. *Biochim. Biophys. Acta.* **1148:** 308–316.
21. Mercadal, M., J. C. Domingo, M. Bermudez, M. Mora, and M. A. De Madariaga. 1995. *N*-Palmitoylphosphatidylethanolamine stabilizes liposomes in the presence of human serum: effect of lipidic composition and system characterization. *Biochim. Biophys. Acta.* **1235:** 281–288.
22. Cravatt, B. F., and A. H. Lichtman. 2003. Fatty acid amide hydrolase: an emerging therapeutic target in the endocannabinoid system. *Curr. Opin. Chem. Biol.* **7:** 469–475.
23. Sun, Y-X., K. Tsuboi, Y. Okamoto, T. Tonai, M. Murakami, I. Kudo, and N. Ueda. 2004. Biosynthesis of anandamide and *N*-palmitoylethanolamine by sequential actions of phospholipase A_2 and lysophospholipase D. *Biochem. J.* **380:** 749–756.
24. Okamoto, Y., J. Morishita, K. Tsuboi, T. Tonai, and N. Ueda. 2004. Molecular characterization of a phospholipase D generating anandamide and its congeners. *J. Biol. Chem.* **279:** 5298–5305.
25. Tsuboi, K., Y-X. Sun, Y. Okamoto, N. Araki, T. Tonai, and N. Ueda. 2005. Molecular characterization of *N*-acylethanolamine-hydrolyzing acid amidase, a novel member of the choloylglycine hydrolase family with structural and functional similarity to acid ceramidase. *J. Biol. Chem.* **280:** 11082–11092.
26. Ramakrishnan, M., V. Sheeba, S. S. Komath, and M. J. Swamy. 1997. Differential scanning calorimetric studies on the thermotropic phase transitions of dry and hydrated forms of *N*-acylethanolamines of even chainlengths. *Biochim. Biophys. Acta.* **1329:** 302–310.
27. Ramakrishnan, M., and M. J. Swamy. 1998. Differential scanning calorimetric studies on the thermotropic phase transitions of *N*-acylethanolamines of odd chainlengths. *Chem. Phys. Lipids.* **94:** 43–51.
28. Swamy, M. J., D. Marsh, and M. Ramakrishnan. 1997. Differential scanning calorimetry of chain-melting phase transitions of *N*-acylphosphatidylethanolamines. *Biophys. J.* **73:** 2556–2564.
29. Ramakrishnan, M., and M. J. Swamy. 1999. Molecular packing and intermolecular interactions in *N*-acylethanolamines: crystal structure of *N*-myristoylethanolamine. *Biochim. Biophys. Acta.* **1418:** 261–267.
30. Ramakrishnan, M., R. Kenoth, R. K. Kamlekar, M. S. Chandra, T. P. Radhakrishnan, and M. J. Swamy. 2002. *N*-Myristoylethanolamine-cholesterol (1:1) complex: first evidence from differential scanning calorimetry, fast-atom-bombardment mass spectrometry and computational modeling. *FEBS Lett.* **531:** 343–347.
31. Swamy, M. J., M. Ramakrishnan, D. Marsh, and U. Würz. 2003. Miscibility and phase behaviour of binary mixtures of *N*-palmitoylethanolamine and dipalmitoylphosphatidylcholine. *Biochim. Biophys. Acta.* **1616:** 174–183.
32. Akoka, S., C. Tellier, C. LeRoux, and D. Marion. 1988. A phosphorus magnetic resonance and a differential scanning calorimetry study of the physical properties of *N*-acylphosphatidylethanolamines in aqueous dispersions. *Chem. Phys. Lipids.* **46:** 43–50.
33. Sheldrick, G. M. 1997. SHELXL97. Program for the Refinement of Crystal Structures. University of Göttingen, Göttingen, Germany.
34. Marsh, D. 1990. Handbook of Lipid Bilayers. CRC Press, Boca Raton, FL.
35. Dahlen, B., I. Pascher, and S. Sundell. 1977. The crystal structure of *N*-(2-hydroxyethyl)-octadecanoate. *Acta Chem. Scand. A.* **31:** 313–320.
36. Larsson, K. 1986. Physical properties—structural and physical characteristics. *In* The Lipid Handbook. F. D. Gunstone, J. L. Harwood, and F. B. Padley, editors. Chapman and Hall, London. 321–384.
37. Wouters, J., S. Vandevoorde, C. Culot, F. Docquir, and D. M. Lambert. 2002. Polymorphism of N-stearoylethanolamine: differential scanning calorimetric, vibrational spectroscopic (FTIR), and crystallographic studies. *Chem. Phys. Lipids.* **119:** 13–21.
38. Abrahamsson, S., B. Dahlén, H. Löfgren, and I. Pascher. 1978. Lateral packing of hydrocarbon chains. *Prog. Chem. Fats Lipids.* **16:** 125–143.
39. Maulik, P. R., M. J. Ruocco, and G. G. Shipley. 1988. Hydrocarbon chain packing modes in lipids: effect of altered sub-cell dimensions and chain rotation. *Chem. Phys. Lipids.* **56:** 123–133.
40. Larsson, K. 1966. The crystal structure of the L-1-monoglyceride of 11-bromodecanoic acid. *Acta Crystallogr.* **21:** 267–272.
41. Goto, M., and T. Takiguchi. 1985. The crystal structure of the β-form of α-monolaurin. *Bull. Chem. Soc. Jpn.* **58:** 1319–1320.
42. Goto, M., K. Kozawa, and T. Uchida. 1988. The crystal structure of the β_1' form of optically active α-monostearin. *Bull. Chem. Soc. Jpn.* **61:** 1434–1436.
43. Pascher, I., M. Lundmark, P. Nyholm, and S. Sundell. 1992. Crystal structures of membrane lipids. *Biochim. Biophys. Acta.* **1113:** 339–372.
44. Pascher, I., S. Sundell, and H. Hauser. 1981. Polar group interaction and molecular packing of membrane lipids. The crystal structure of lysophosphatidylethanolamine. *J. Mol. Biol.* **153:** 807–824.
45. Pascher, I., and S. Sundell. 1985. Interactions and space requirements of the phosphate head group in membrane lipids. The crystal structure of disodium lysophosphatidate dihydrate. *Chem. Phys. Lipids.* **37:** 241–250.